Physica Scripta

REPLY

Effect of dielectric mismatch on impurity binding energy, photoionization cross-section and stark shift of CdS/ZnSe core shell spherical quantum dots

A Cherni[1], N Yahyaoui[1], N Zeiri[1,*], P Baser[2], M Said[1] and S Saadaoui[3]

[1] Laboratory of Condensed Matter and Nanosciences (LMCN) Department of Physics, Faculty of Sciences of Monastir, 5019 Monastir, Tunisia
[2] Sivas Cumhuriyet University, Turkey
[3] Department of Physics, Faculty of Science and Arts, Mohayel Aser, King Khalid University, Abha, Saudi Arabia
[*] Author to whom any correspondence should be addressed.

E-mail: zeirinabil@gmail.com

Keywords: hydrogenic impurity, electric field, binding energy, stark shift, PICS, core/shell QDs

RECEIVED
1 March 2023

REVISED
12 May 2023

ACCEPTED FOR PUBLICATION
8 June 2023

PUBLISHED
5 July 2023

Abstract

The variational approach has been used to investigate theoretically the effects of the dot radius and electric filed strength on binding energy (BE), Stark-shift and photoionization-cross section (PICS) of donor impurity confined in the (CdS/ZnSe) core/shell spherical quantum dot (CSSQDs) capped in different dielectric matrices such as the silicon dioxide (SiO_2), the polyvinyl chloride (PVC) and the polyvinyl alcohol (PVA). Our achieved results showed that the BE and the Stark shift depended highly on the presence of the dielectric matrix and the modification of the core radius. The increase of applied electric field (EF) intensity and the core radius induces a decrease in the BE and lead to an improvement of (PICS) magnitude accompanied by the redshift of their resonance peaks.

Introduction

Low-dimensional systems (LDS) are generally classified into three groups based on their confinement size. Two-dimensional (2D) systems containing thin films, layer structures and quantum wells in which particle movement is limited to one dimension. One-dimensional (1D) systems such as semiconductor wires and linear chain-like structures in which particle movement is limited o two dimensions, and three dimensions of particle motion zero-dimensional (0D) systems such as quantum dots and colloids [1]. Quantum dots are known as LDS structures with atom-like dirac delta functional state density.Therefore, these structures are also called 'artificial atoms' [2]. The size of a QD is typically considered to be between 1 and 20 nm [3]. At such small scales, QDs have been seen to exhibit molecule-like behavior by interacting with light via electronic transition dipoles [4]. Quantum dots are used in many technology areas due to their unique optical properties such as high brightness and narrow emission band, and their advantages over other low-dimensional systems. For example, in immunoassays, microarrays, fluorescent imaging applications, quenching sensors and barcoding systems [5, 6], QD probes can be used as biosensors in nanomedicine to target and detect cancer cells [7]. In addition, some of the uses of quantum dots can be listed as energy storage [8–10], solar cell energy conversion [11], photodetector [12], quantum computing [13], quantum dot vertical cavity surface emitting lasers (VCSELs) [14]. It has also been shown to provide remarkable advantages in the design of many optoelectronic devices, such as the intersublevel photodetector (QDIP) [15]. The evolution of performances of these nanostructures has taken the opportunity of the progress made by the different growth methods which give the possibility to modify the size, shape, and material composition of QDs to adjust the intersubband resonance frequency and improve their optical proprieties. Recently, distinct theoretical and experimental research has been focused on studying the linear and nonlinear optical proprieties and energy states of a single electron confined in QDs [16–21]. It was shown by P Anchalah *et al* [21] that the presence of different dielectric matrices ensures chemical stability and

improves the optical properties of Si QDs. In quantum dots, as in other low-dimensional structures, the shape of the encompassement potential of the particles has an important effect as it determines the optical performance of the structure [22]. Some experimental studies have suggested that the optimal quantum dot profiles to contain electrons should be well-like [23]. Within this experimental suggestion, this article focused on the square well potential. Coating the quantum dot core with different bandgap semiconductor material creates a unique category known as core–shell quantum dots (CSQDs) [24–28]. Core/shell quantum dot systems (CSQDs) are one of the greatest models for new fields in nanotechnology applications thanks to their exceptional physical proprieties such as three-dimensional quantum confinement of charge carriers and discretization of the energy spectrum. It was studied that the shell around the nucleus provides chemical stability to the nucleus and reduces non-radiative recombination resulting in high quantum efficiency [29].

In addition, the optical properties of these CSQDs can be adjusted by modifying the shell thickness and doping [30]. These CSQDs are attracting considerable attention for optoelectronic device designs due to their tunable transition energies [31]. The size dependent variation of the transition energy of the CSQD was found to improve the range of the absorption and emission spectrum [32]. Due to the relative band alignment of the core and shell composite, the shell around the core increases the enveloping effect of the carriers, resulting in increased PL efficiency compared to shellless QDs [33]. The outer shell protects the structure of the nucleus by preventing the potential changing of free heavy metal ions, and optical and electronic properties can be changed by doping these quantum dots [34]. One of the major problems with using these structures for optoelectronic devices is how to matrix them into a medium such as glasses and polymers to form a composite that can be easily used for applications [35–37]. Providing a suitable matrix selection, highly stable luminescent materials can be obtained due to passivation of the surface states of the quantum dot through the interaction of the matrix elements. PVA (poly-vinyl alcohol) [38], PMMA (poly-methyl methacrylate) [39], PVC (poly-vinyl chloride) [40], and SiO_2 (silicon dioxide) can be used [41]. PVA proved to be a good polymeric host matrix of choice in quantum dot materials such as CdS and polymers based on different potential nanohybrid composites [42]. CdS-containing QDs were chosen as an optimum material because of their attractive optical properties such as photo stability, size-dependent band gap, optical absorption in the UV region, and bright photoluminescence (PL). Addition of nanoscale inorganic fillers to polymers and obtaining polymer nanocomposites with superior properties have been the focus of attention of many researchers in recent years. The most important properties of CdS encapsulated with PVC matrix, such as thermal, optical, mechanical and antibacterial, were also proven to significantly improve the optical properties of the material [43]. It is important to examine the dielectric effect in low-dimensional systems. Because the dielectric screening reduces the possibility of scattering and capture of charge carriers by imperfections. Therefore, it was found to be an important variable parameter in improving the photoelectric conversion performance and carrier transitions in semiconductors [44]. Core/shell quantum dot (CSQDs) structures were observed to exhibit interesting optical and electrical properties due to being surrounded by materials with dielectric mismatch. For example, it was found that the dielectric screening of core–shell QDs is geometry dependent, and the dielectric effect of CdSe/CdS QDs can be tuned by changes in the Auger ratio [45]. It was proved that as the dielectric constant ratio between materials increased, the exciton binding energy and exciton oscillator power increased significantly and the change in dielectric constant had a significant effect on the emission properties of the CdSe quantum dot [46, 47]. Therefore, the elucidation of dielectric confinement effects in core–shell structures is of great interest for new device designs. In this study, the dependence of shallow donor binding energy and PICS on the geometry of the system and the matrices surrounding the structure in CdS/ZnSe core/shell quantum dot confinement by different dielectric matrices such as SiO_2, PVC and PVA are detailed. With the advancement of crystal growth techniques, spherical [48], cube [49], prism [50], hexagonal [51], disc [52] shaped CSQDs were obtained. Different shapes of CSQDs have been shown to have many optoelectronic applications such as solar cells [53], light-emitting diodes (LEDs) [54], luminescent solar concentrators (LSCs) [55], optical detectors [56].

In this study, the CSQD structure obtained from CdS/ZnSe semiconductors consisting of a spherical core and a spherical semiconductor shell was investigated. In addition, in the field of nanostructure systems, the study of impurity energy states in QDs has played an important role in improving the electronic properties of semiconductor nanomaterials and improving the electronic, optical and thermal properties of QD-based devices and has become the most basic requirement in low-dimensional systems where optical transition can occur between the ground state of donor impurity and the conduction subband. In addition, since it changes the effective potential profile of the external electric field applied to the structure, it can be used as a tuning parameter on the electronic and optical properties of the structure. For this reason, many theoretical and experimental studies have been carried out on quantum dots under electric field or containing impurities [57–61]. The optical properties of the CdS/ZnS core/shell spherical quantum dot for the central donor impurity under the electric and magnetic field were calculated by K Hasanirokh *et al.* It was observed that the transition energy decreased as the core radius and external magnetic field increased, thus the resonance peaks were redshifted. It was also proved that the resonance peaks were blue-shifted when the applied electric field intensity

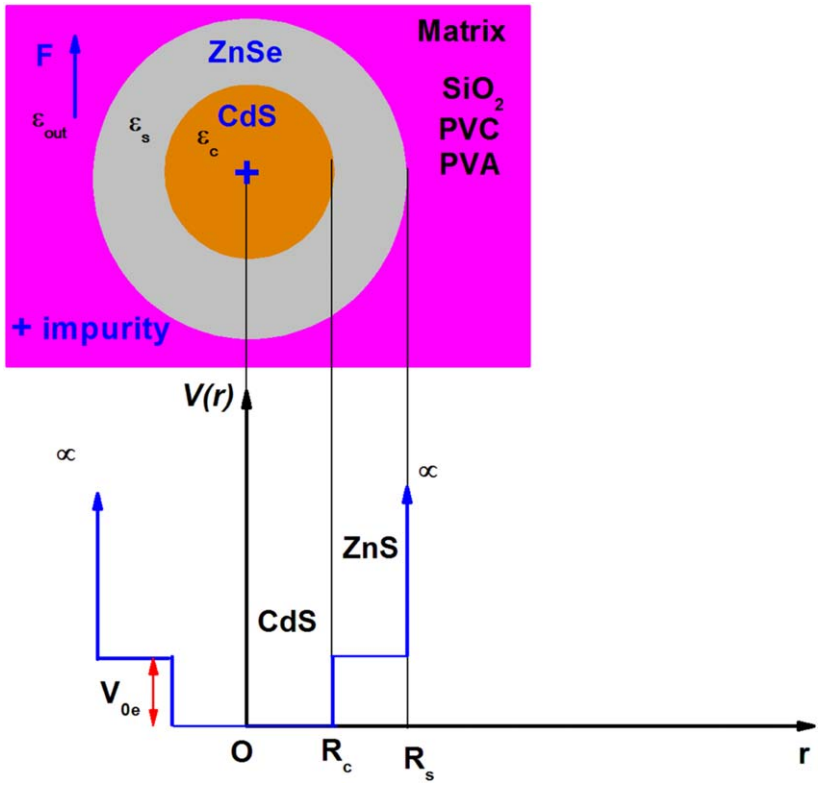

Figure 1. Schematic plot of CdS/ZnSe CSQDs coated by different matrices.

was increased [62]. On the other hand, the BE of shallow donors and acceptors in spherical GaAs/Al1-xGaxAs QDs for both a finite barrier and an infinitely high barrier was studied by Zhen-Yan Deng *et al* Dielectric screening has been proven to increase the binding energy for the central shallow donor and acceptor ion, especially as the dot radius decreases [63]. The binding energy and photoionization fraction (PICS) of the hydrogen impurity have been studied by many authors depending on the external EF and QD size [64–68]. L Shi *et al* [64] calculated the binding energy of a donor impurity trapped in a non-axial elliptical cylindrical core/shell quantum dot (ECCSQD) using a variational and perturbation approach. The variation of core and shell dimensions, ellipticity constant, binding energy and photoionization cross section (PCS) depending on the impurity position under an axial electric field were investigated. The binding energy in an elliptical cylindrical core/shell quantum dot was shown by the authors to be lower than in a cylindrical core/shell quantum dot. It has also been proven that the elliptical cylinder shape has a significant effect on the peak density and position of the PICS.

Using effective mass approach and variational technique, the binding energy and photoionization cross section of shallow donor impurities in GaAs/GaAlAs parabolic quantum wire under the influence of electricity and intense laser fields were theoretically investigated by U Yeşilgül [68]. The binding energy and PCIS were found to depend largely on the size of the wire, the electric field, and the intense laser field. It was observed that the impurity binding energy decreased with increasing electric field. It was observed that the binding energy was more sensitive to the external electric field as the wire size increased. In addition, it was observed that the size of the PICS increased as the electric field increased, as the Coulomb interaction between the electron and the donor impurity decreased as the electric field increased.

In section 2, we have introduced a theoretical formulation allowing us to calculate the BE of the ground state, the corresponding wave functions and PICS of on-center impurity confined in CdS/ZnSe CSQDs embedded in different dielectric matrices. The obtained results and their discussions are presented in section 3. Finally, the main results are recapped in section 4.

Theory and calculation

The Hamiltonian equation is solved for the central donor impurity ion in CdS/ZnSe spherical CSQDs under electric field, coated with different dielectric matrices such as SiO_2, PVA and PVC. The applied electric field ($\vec{F}_z$) is in the z direction. Figure 1 shows the schematic diagram of CdS/ZnSe CSQDs coated with different matrices and the variation of confinement potential with radial distance. The dimensions of the core and outer shell are

Rc and Rs, respectively. V_{0e} is the electron confinement potential due to the conduction band discontinuity. Under the effective mass and parabolic band approach, the Hamiltonian of CdS/ZnSe spherical CSQDs under an electric field containing a single electron and donor impurity is defined as follows [69]:

$$(\hat{H}_0 + \widehat{H'})\Psi_{n,l}(\vec{r}) = E_{n,l}(\vec{r})\Psi_{n,l}(\vec{r}) \tag{1}$$

$\hat{H}_0$ is the Hamiltonian of the single electron confined in (CdS/ZnSe) spherical QDs/Matrix without impurity and in absence of the EF, expressed as follow:

$$\hat{H}_0 = \frac{-\hbar^2}{2}\vec{\nabla}\left(\frac{1}{m_i^*}\vec{\nabla}\right) + V_{conf}(\vec{r}) + \sum(R_s) \tag{2}$$

Here, the first term is the kinetic energy operator for the electron, the effective mass of an electron in the region i^{th} (core or shell) is m_i^* and $V_{conf}(\vec{r})$ is the spatial confinement potential. The $V_{conf}(\vec{r})$ is defined as

$$V_{conf}(\vec{r}) = \begin{cases} 0 & 0 \leqslant r \leqslant R_c \\ V_{0e} & R_c \leqslant r \leqslant R_s \\ \infty & r \geqslant R_s \end{cases} \tag{3}$$

And $\sum(R_s)$ designate the self-polarization potential induced by the external dielectric medium, expressed as [21]:

$$\sum(R_s) = \frac{e^2}{4\pi\varepsilon_0 R_s}\left[\frac{1}{2}\left(\frac{1}{\varepsilon_{out}} - \frac{1}{\varepsilon_{in}}\right) + \frac{0.466}{\varepsilon_{in}}\left(\frac{\varepsilon_{in} - \varepsilon_{out}}{\varepsilon_{in} + \varepsilon_{out}}\right)\right] \tag{4}$$

ε_0 is the permittivity in vacuum, $\varepsilon_{in} = \sqrt{\varepsilon_{CdS}.\varepsilon_{ZnSe}}$ and ε_{out} are respectively the permittivity of CdS/ZnSe CSQDs and the dielectric matrix. In equation (1), $\widehat{H'}$ is considered as the perturbation Hamiltonian including the effects of Coulombic potential and external EF, given by:

$$\widehat{H'} = U(\vec{r}) + eF.r.\cos(\theta) \tag{5}$$

e is the elementary charge of the electron and U(r) is the potential energy given as the sum of the interaction of the electron with the impurity and the polarization charges [70]. Here r is the electron-impurity distance.

$$U(\vec{r}) = -\frac{e^2}{4\pi\varepsilon_{in} r} - \frac{e^2(\varepsilon_{in} - \varepsilon_{out})}{4\pi\varepsilon_{in}\varepsilon_{out} R_s} \tag{6}$$

In the absence of electric field and without impurity, the wave functions of $\hat{H}_0$ can be written in a spherical coordinates system as $\Psi^0_{n,l}(r, \theta, \varphi) = R^0_{n,l}(r).Y_{l,m}(\theta, \varphi)$, with $Y_{l,m}(\theta, \varphi)$ are the spherical harmonics and $R_{n,l}(r)$ is the radial part taken from [71]:

$$R^0_{n,l}(r) = \begin{cases} A_1 J_l(k_{nl,1}.r) & 0 \leqslant r \leqslant R_c \\ B_1 h_l^+(ik_{nl,1}.r) + B_2 h_l^-(ik_{nl,2}.r) & R_c \leqslant r \leqslant R_s \\ 0 & r \geqslant R_s \end{cases} \tag{7}$$

Ben Daniel-Duke boundary conditions were applied to the wave functions to satisfy the quantum mechanical continuity condition. Normalization constants A_1, B_1 and B_2 can be determined from these boundary conditions [71, 72]. The coefficients $k_{nl,1}$ and $k_{nl,2}$ depending on the electronic energy value in equation (7) are given by equation (8).

$$k_{nl,1} = \frac{\sqrt{2m^*_{CdS}(E_{n,l} - \sum(R_s))}}{\hbar^2},$$
$$k_{nl,2} = \frac{\sqrt{2m^*_{ZnSe}(V_c + \sum(R_s) - E_{n,l})}}{\hbar^2} \tag{8}$$

The contribution of Coulomb potential and EF strength in equation (1) required the use of a variational method to compute the impurity ground state energy. The trial function $R_{\lambda,\eta}(r)$ associate to the impurity ground state is taken from [72]:

$$R_{\lambda,\eta}(r) = R^0_{n,l}(r)e^{-\lambda r}e^{-\eta r\cos\theta} \tag{9}$$

In equation (9), λ and η are the variational parameters introduced to assume respectively the corrections made by the Colombic potential and the impact of the external EF. Considering the perturbation theory, the ground state energy of impurity must satisfy the following condition [66, 72, 73] concerning λ and η:

$$E = \min_{\lambda,\eta}\frac{\langle\Psi_{n,l}(r, \theta, \varphi)|\hat{H}|\ \Psi_{n,l}(r, \theta, \varphi)\rangle}{\langle\Psi_{n,l}(r, \theta, \varphi)|\ \Psi_{n,l}(r, \theta, \varphi)\rangle} \tag{10}$$

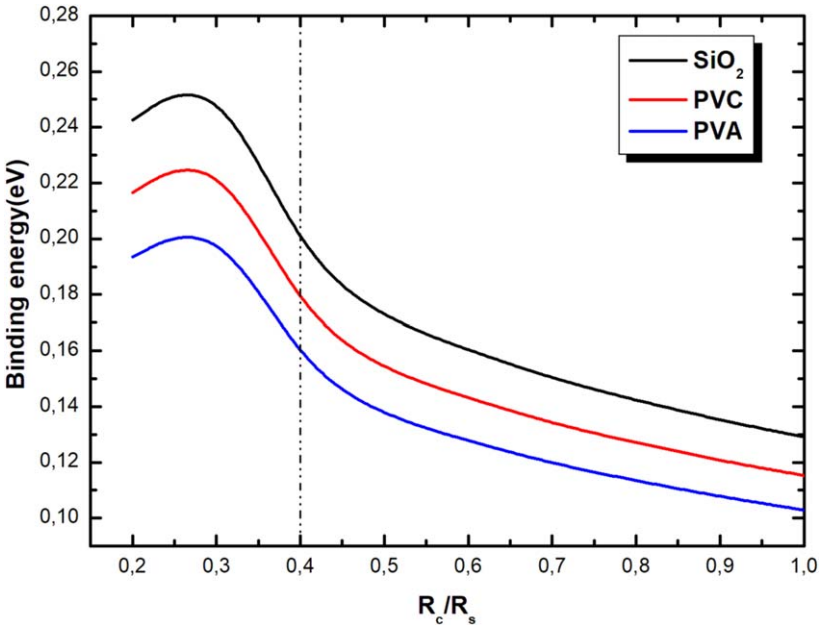

Figure 2. The variation of ground state BE as a function of core-to-shell radii ratio R_c/R_s for different dielectric matrices: PVA, PVC and SiO_2 with $R_s = 5$ nm.

Where $\hat{H}$ is the total Hamiltonian. The BE is defined as the difference between the ground state energies without and with impurity [74]:

$$E_b = E_0 - E \tag{11}$$

The PICS defines the probability of ionization of the electron attached to a hydrogenic impurity by the effect of external photon excitation. In this study, we considered the PICS describing the optical transition between ground states with and without impurity. The expression given PICS variation is given in the dipole approximation as [75–78]:

$$\sigma(\hbar\omega) = \left[\left(\frac{F_{eff}}{F_0}\right)^2 \frac{n_r}{\varepsilon_{in}}\right] \frac{4\pi^2}{3} \beta_{FS} \hbar\omega \sum_f |M_{if}|^2 \delta(\Delta E_{if} - \hbar\omega) \tag{12}$$

In the above equation, $n_r = \sqrt{\varepsilon_{in}}$ is the refractive index of QDs, $\hbar\omega$ represents the incident photon energy, F_{eff} and F_0 are the incident effective field and average field in the medium respectively in which the ratio $\frac{F_{eff}}{F_0}$ is taken equal 1 for the reason that it does not affect PICS shape, $\beta_{FS} = \frac{e^2}{4\pi\varepsilon_0\hbar c}$ is the fine structure parameters, ΔE_{if} represent the difference in energy. $M_{if} = F\Psi_i|r|\ \Psi_f$ designate the dipole matrix element, Ψ_i and Ψ_f are the initial and final eigenwave functions with and without impurity givens respectively by equation (1) and (2). F is a dimensionless factor describing the discontinuity of EF inside and outside the (QD) given by [79]:

$$F = \frac{3\varepsilon_{out}}{\varepsilon_{in} + 2\varepsilon_{out}} \tag{13}$$

And $\delta(\Delta E_{if} - \hbar\omega)$ is the Lorentzian function given by:

$$\delta(\Delta E_{if} - \hbar\omega) = \frac{\hbar\Gamma}{\pi[(\hbar\omega - (\Delta E_{if}))^2 + (\hbar\Gamma)^2]} \tag{14}$$

Where $\Gamma = \frac{1}{\tau}$ is the hydrogenic impurity line width.

Result and discussion

In this study, we compute and perform the BE, stark shift and PICS of the on-center impurity in CdS/ZnSe spherical QDs immersed in various dielectric mediums. The material parameters used in our calculation are: The effective mass is $m^*_{CdS} = 0.19m_0$, $m^*_{ZnSe} = 0.15m_0$ [79, 80] and the electron confinement potential is $V_{0e} = 0.8$ eV. $E_g(CdS) = 2.49$ eV and $E_g(ZnSe) = 2.69$ eVare the bangap energy for CdS and ZnSe, respectively [81]. The dielectric constants of the material in the core–shell QD structure are given as $\varepsilon_{CdS} = 5.50$ and

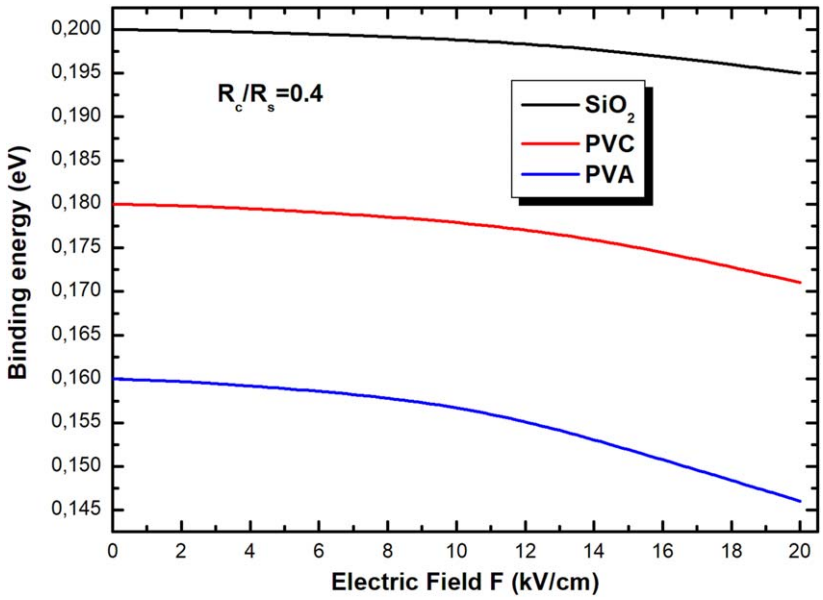

Figure 3. The variation of ground state BE versus the applied EF strength for different dielectric matrices and a fixed ratio $R_c/R_s = 0.4$ with $R_s = 5$ nm.

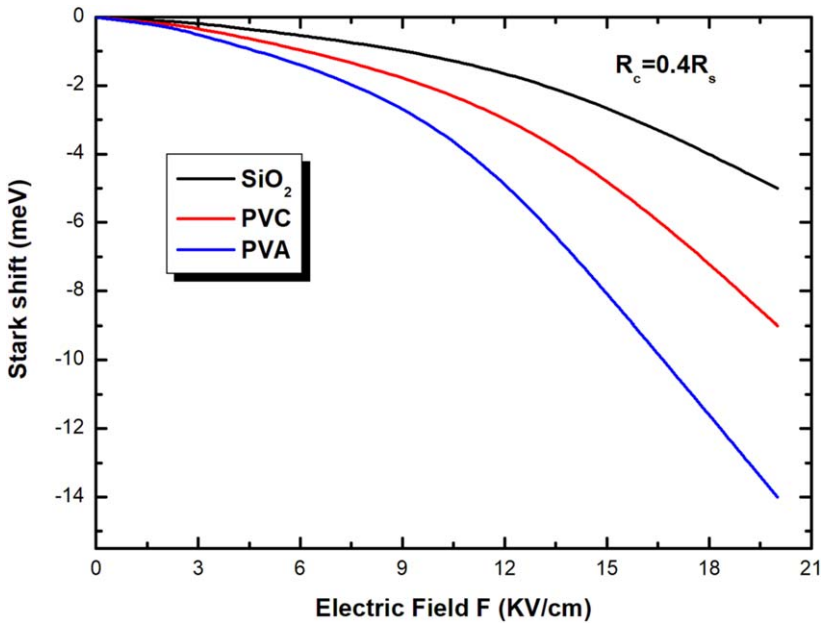

Figure 4. The variation of the Stark-shift versus EF strength for different dielectric matrices and for a fixed ratio $R_c/R_s = 0.4$ with $R_s = 5$ nm.

$\varepsilon_{ZnSe} = 5.23$ respectively [82]. The dielectric constant of CdS/ZnSe (QDs) is $\varepsilon_{in} = \sqrt{\varepsilon_{CdS}.\varepsilon_{ZnSe}} = 5.36$ and that of SiO_2, PVC and PVA mediums are 3.9, 4.6 and 14 respectively [83, 84]. Outer radius for CdS/ZnSe core–shell quantum dots R = 7 nm up to nm. This value is slightly larger than from the bulk CdS Bohr radious ($a_B = \hbar^2\varepsilon_{CdS}/m^*_{CdS}e^2 \sim 1.46$ nm). The reason for choosing this size is that when the quantum confinement effects are comparable, characteristic of the impurity, Coulomb interaction, polarization charges induced at the interface can be observed.

In figure 2, we present the dependence of BE on the core–shell radius ratio R_c/R_s for the ground state for three different dielectric media, SiO_2, PVC and PVA. From this figure, we can say that BE is strongly sensitive to core size change. As R_c/R_s decreases, BE starts to increase as the electron and impurity move close to each other. BE reaches a maximum with decreasing Rc/Rs value and starts to decrease after a certain value ($R_c/R_s = 0.1$).The reason for this is that after this value of the Rc/Rs ratio, since the size of the CSQD becomes very small, the electron becomes very energetic and leaks into the shell region consisting of ZnSe, in this case BE decreases as it

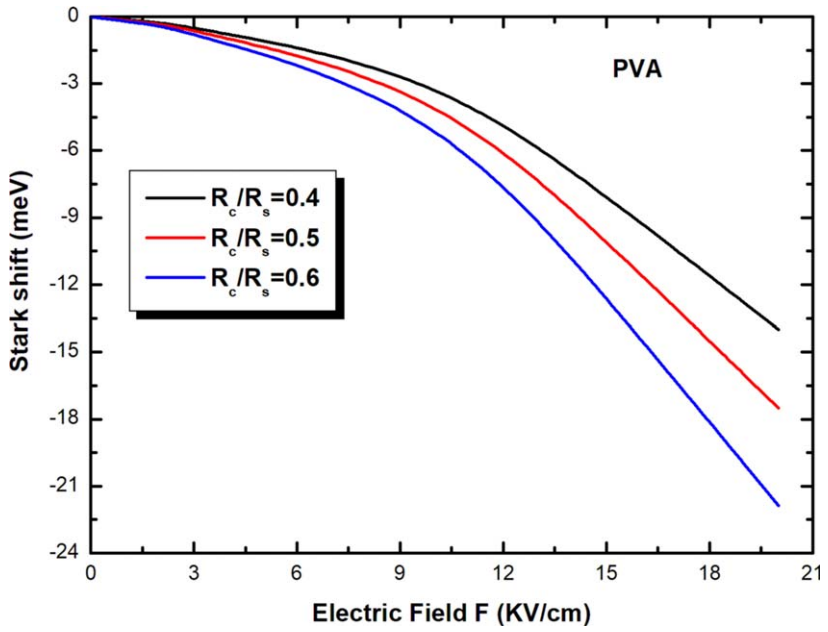

Figure 5. The dependence of the Stark shift on the EF strength for different core radii in the case of the PVA matrix.

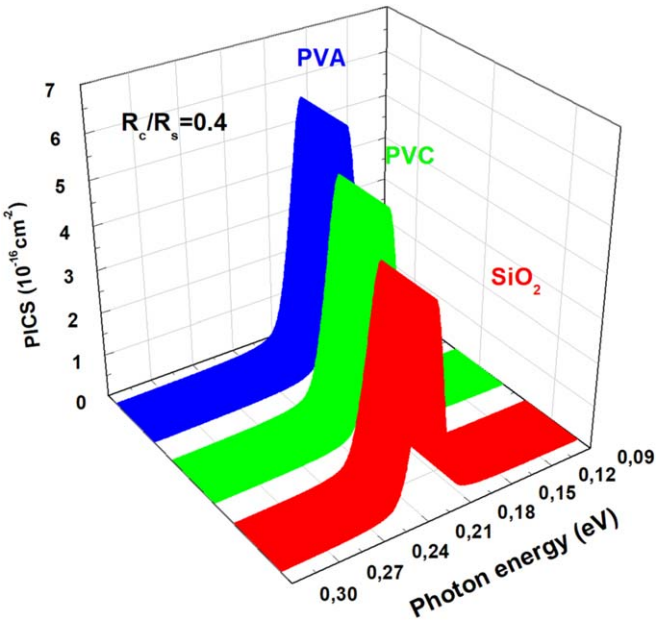

Figure 6. The dependence of the PICS on the incident energy photon for different dielectric matrices and the fixed value core radius $R_c = 0.4R_s$ with $R_s = 5$ nm.

moves away from the impurity ion. In other words, the maximum value of BE coincides with the ratio $R_c/R_s = 0.1$, where the distance between the impurity and the electron reaches its minimum. Therefore, as the R_c core size changes, BE also changes due to the change in the electron-impurity distance. From this we can say that the binding energy is directly related to the core size. The dielectric confinement effect creates an extra confinement for the system, reducing the stability of the structure, resulting in lower electronic energy levels. In other words, it modifies the Coulomb interaction by shielding, significantly reducing it, leading to lower binding energies. Our results are in good agreement with other studies [69, 85, 86]. For example, in the PVA matrix with the highest dielectric constant, the maximum value of BE is around 160 meV. (See figure 2). Whereas, the value of BE for the central donor impurity in the core–shell nanoparticle without dielectric is around 650 meV. The final point to note in figure 2 is that the change of BE strongly depends on the nature of the matrix in which QD is embedded. For example, considering the maximum values of BE at $R_c/R_s = 0.1$, it is $E_b = 0.2$ eV for SiO_2 matrix, $E_b = 0.18$ eV, for PVC matrix, and $E_b = 0.16$ eV for PVA matrix. Our results are in good agreement with

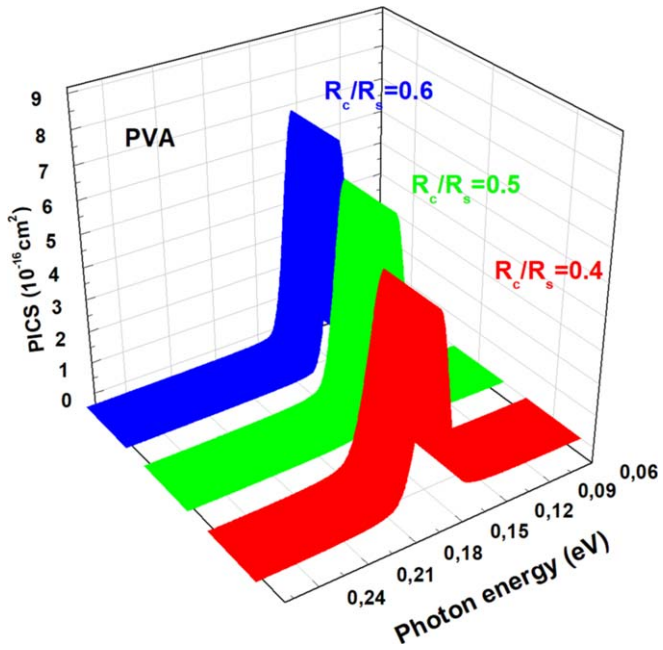

Figure 7. The dependence of the PICS on the incident energy photon for the different core radius in the case of the PVA matrix with $R_s = 5$ nm.

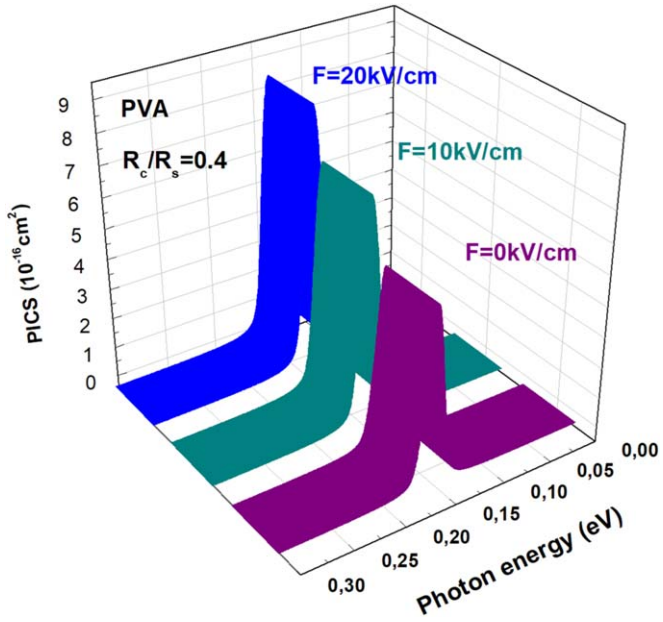

Figure 8. The PICS variation as a function of incident energy photon for different EF strengths in for a fixed core radius $R_c = 0.4R_s$ and in the case of PVA matrix with $R_s = 5$ nm.

other studies [87, 88]. Adjusting the quantum dot size and appropriate selection of the dielectric medium offers the possibility to modulate the energy transition in a QD-matrix system.

Figure 3 presents the dependence of BE on EF strength for a constant core–shell radius ratio for different dielectric media. It is seen that BE is strongly affected by the applied EF strength for all dielectric environments, and BE decreases as the applied EF increases. This is because the applied EF strength breaks the symmetry of the confinement potential. In this case, as the electric field increases, the Coulomb interaction between electron and donor impurity decreases, so the impurity binding energy decreases. Our results are in good agreement with those in reference [89]. When the authors investigated the effect of EF on BE of the central impurity in a $GaAs/Ga_{0.7}Al_{0.3}As$ core–shell spherical QD with parabolic symmetry potential, they proved that the applied EF changes the spatial distribution of the electron and the Coulomb interaction decreases.

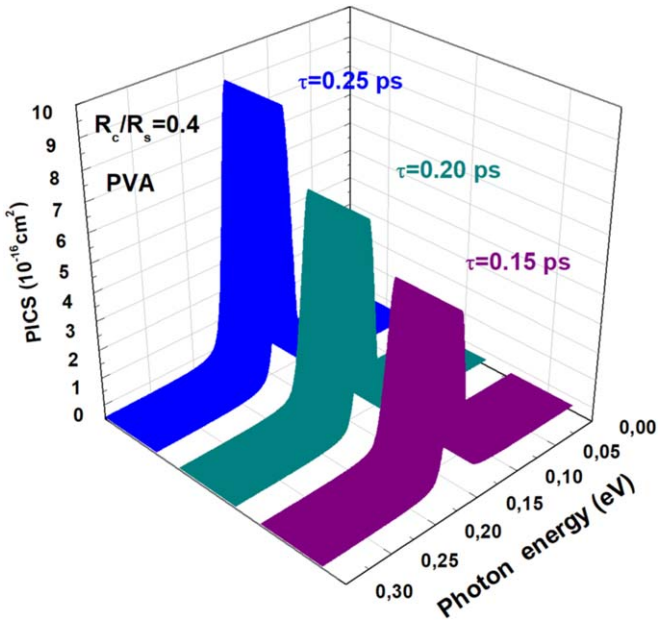

Figure 9. The PICS variation versus incident energy photon for different relaxation times for the fixed value of core radius $R_c = 0.4R_s$ and in the case of the PVA matrix with $R_s = 5$ nm.

In figure 4, we present the variation of the stark shift dependent on the applied EF strength to explain the effect of the external EF strength on BE. Results are determined for three dielectric mediums and constant core–shell radius ratio $R_c/R_s = 0.4$. The Stark shift is defined as the difference (DE) between electronic energies with and without an electric field [73]. In the case of SiO_2 medium with lower dielectric constant $\varepsilon_{out} = 3.9$, we can say that by increasing the applied EF strength, the stark shift is less than in PVC and PVA matrix mediums with large dielectric constant. Because the Coulombic potential effect is stronger when the dielectric effect is weak, the charge distribution is less sensitive to the electric field. In all three of the SiO_2, PVC, and PVA matrices, the stark shift becomes more pronounced and more significant as the electric field increases, because as the electric field increases, the Coulomb interaction decreases as the electron and the impurity move away from each other. This causes the binding energy to decrease with increasing electric field. From the results we have obtained, we can say that as the dielectric constant of the matrix surrounding the core–shell QDs decreases, the variation of the stark shift with the electric field will weaken due to the weak confinement effect.

We have illustrated in figure 5 the stark shift versus EF intensity for three sizes of the core radius in the case of the PVA medium. As shown in this figure, the stark shift is not only affected by EF but also by the geometric factor. It can be noted that the stark shift has a parabolic variation which increases with increasing the core radius. For the smaller QDs size, the stark shift is less sensitive to EF intensity due to the quantum effect. Our analyses are in good agreement with [90].

We have depicted in figure 6 the variation of the PICS in terms of incident photon energy with a fixed core-to-shell radius ratio $R_c/R_s = 0.4$ without EF and for three different mediums. It can be seen that the PICS increase and their resonance peak intensity shift to lower energy in the case of QDs/PVA, in this case $\varepsilon_{out} > \varepsilon_{in}$, the local field factor $F > 1$ which induces an increase in the transition matrix element $M_{i,j}$ and giving a stronger PICS magnitude result in a better overlap between wave functions. Otherwise, when $\varepsilon_{out} < \varepsilon_{in}$, the dipole matrix element $M_{i,j}$ decreases and generates a lower magnitude. In figure 7, we have presented the impact of the core radius on PICS, the calculations are performed in the case of PVA medium. From this figure, it should be noted that with an increase in the core radius, the resonance peaks move to lower energies with an improvement of PICS magnitude due to an increase of the $M_{i,j}$ element. L Shi *et al* [91] have obtained the same behavior with different shapes of CSQDs.

The influence of the EF in such core–shell nanostructures has broken the spherical symmetry of the confinement potentials which ensures the modification of the energy levels and the overlap of the wave functions which will in turn improve the optical properties. In figure 8, we have illustrated the dependence of the PICS on the applied EF intensity in the case of the PVA matrix for the fixed value of the core radius. According to the results shown in figure 3, the increase in EF intensity led to a decrease in the BE and the resonance peaks of the PICS exhibit a redshift. On the other hand, the increasing EF strength gives rise to the electron-impurity distance

thus the $M_{i,j}$ element increases which improves the PICS magnitude. Our achieved results are in agreement with those found in [66, 87].

In figure 9 we have plotted the PICS versus photon energy for a fixed core radius $R_c = 0.4R_s$ in the case of the PVA matrix for three distinct values of relaxation time. From this figure, one can be seen that when the relaxation time increases from 0.15ps to 0.25ps, the PICS magnitude presented a significant rise from 5.75 10^{-16} cm^2 to 9.4 10^{-16} cm^2 with keeping the resonance picks energy close to 0.16 eV while the core radius is fixed [89–91]. This result has an important impact on improving the performance of optoelectronic and photonic devices.

Conclusion

In this study, the perturbation method has been used under the framework of the effective mass approximation to investigate the combined effects of dielectric matrix, geometric factors and the applied EF on the BE, Stark-shift and PICS of hydrogenic impurity located on the center of CdS/ZnSe spherical QDs. The numerical results proved that the quantum confinement effect and the dielectric mismatch between the QDs and capped matrix play an important role in the BE optimization and the stability of impurity. Moreover, it is noted that the PICS magnitude is strongly affected by the applied electric field intensity and geometric factors. Our theoretical results showed that the increased EF strength and core radius enhanced the PICS intensity with a redshift of resonance peaks. Additionally, the peak magnitude increases with the relaxation time while keeping the resonance energy. This study shows that the desired energy range for impurity levels in heterostructures modulated with dielectric medium under electric field, hence the binding energy, can be adjusted by changing the dielectric constant, structure parameters and electric field of the capped matrices. From here, we think that new optoelectronic devices can be designed by adjusting the dielectric confinement effect and will contribute to experimental studies with a practical application method.

Acknowledgments

The authors extend their appreciation to the Deanship of Scientific Research at King Khalid University for funding this work through large group Research Project under grant number RGP2/19/44.

Data availability statement

The data cannot be made publicly available upon publication because no suitable repository exists for hosting data in this field of study. The data that support the findings of this study are available upon reasonable request from the authors.

ORCID iDs

N Yahyaoui https://orcid.org/0000-0002-3677-6180
N Zeiri https://orcid.org/0000-0003-3050-8262

References

[1] Yoffe A D 2002 *Adv. Phys.* **51** 799–890
[2] Maksym P A and Chakraborty T 1990 *Phys. Rev. Lett.* **65** 108–11
[3] Nirmal M and Brus L 1999 *Acc. Chem. Res.* **32** 407–14
[4] Alivisatos A P 1996 *Science* **271** 933–7
[5] Zhang Y and Wang T H 2012 *Theranostics.* **2** 631–54
[6] Mansuriya B D and Altintas Z 2020 *Sensors* **20** 1072(1)–1072(71)
[7] Iannazzo D, Espro C, Celesti C, Ferlazzo A and Neri G 2021 *Cancers.* **13** 3194(1)–3194(15)
[8] Hoang V C, Dave K and Gomes V G 2019 *Nano Energy.* **66** 104093(1)–104093(18)
[9] Zahir N, Magri P, Luo W, Gaumet J J and Pierrat P 2022 *Energy & Environmental Materials. 5* 201–14
[10] Huang R, Wang L, Zhang Q, Chen Z, Li Z, Pan D, Zhao B, Wu M, Wu C M L and Shek C H 2015 *ACS Nano.* **9** 11351–61
[11] Yao D, Hu Z, Zheng L, Chen S, Lü W and Xu H 2023 *Appl. Surf. Sci.* **608** 155230(1)–155230(6)
[12] Clifford J P, Konstantatos G, Johnston K W, Hoogland S, Levina L and Sargent E H 2009 *Nat. Nanotechnol.* **4** 40–4
[13] Loss D and DiVincenzo D P 1998 *Phys. Rev.* A **57** 120
[14] Sheikhey M M, Mahjoory A, Baghban H and Golmohammadi S 2022 *Appl. Opt.* **6** 1523–30
[15] Lagraa I, Soudini B, Abid H and Taleb S 2022 *Optik* **251** 168494(1)–168494(8)
[16] Máthé L, Onyenegecha C P, Farcaş A-A, Pioraş-Ţimbolmaş L M, Solaimani M and Hassanabadi H 2021 *Phys. Lett.* A **397** 127262(1)–127262(10)

[17] Yamijala S S R K C, Mukhopadhyay M and Pati S K 2015 *J. Phys. Chem. C* **119** 12079–87
[18] Srinivasan K and Painter O 2007 *Nature* **450** 862–5
[19] Kim S H, Man M T, Lee J W, Park K D and Lee H S 2020 *Nanomaterials.* **10** 1589(1)–1589(9)
[20] Fonoberov V A, Pokatilov E P and Balandin A A 2002 *Phys. Rev.* B **66** 085310(1)–085310(13)
[21] Purohit A S P and Mathur K C 2011 *J. Appl. Phys.* **110** 114320(1)–114320(8)
[22] Bera S M A A, Ghosh A and Ghosh M 2020 *Physica* B **588** 412166
[23] Davies J H 1999 *The Physics of Low-Dimensional Semiconductors: An Introduction* 5 edn (Cambridge, USA)
[24] Mews A, Eychmueller A, Giersig M, Schooss D and Weller H 1994 *J. Phys. Chem.* **98** 934–41
[25] Haus J W, Zhou H S, Honma I and Komiyama H 1993 *Phys. Rev.* **47** 1359–65
[26] El Haouari M, Talbi A, Feddi E, El Ghazi H, Oukerroum A and Dujardin F 2017 *Opt. Commun.* **383** 231–7
[27] Hines M A and Guyot-Sionnest P 1996 *J. Phys. Chem.* **100** 468–71
[28] Toscano-Negrette R G *et al* 2023 *Nanomaterials.* **13** 550(1)–550(18)
[29] Hasanirok K, Radu A and Duque C A 2022 *Nanomaterials.* **12** 4014(1)–4014(22)
[30] Wang L, Wang J, Su X and Chen R 2022 *J. Alloy. Compd.* **920** 165907
[31] Feng X, Xiong G, Zhang X and Gao H 2006 *Phys. B Condens. Matter.* **383** 207–12
[32] Woon C Y, Gopir G and Othman A P 2011 *Sains Malaysiana.* **40** 55–8
[33] Vasudevan D, Gaddam R R, Trinchi A and Cole I 2015 *J. Alloy. Compd.* **636** 395–404
[34] Sahu A and Kumar D 2022 *J. Alloys Compd.* **924** 166508(1)–166508(22)
[35] Schlamp M C, Peng X and Alivisatos A P 1997 *J. Appl. Phys.* **82** 5837–42
[36] Gao M, Richter B, Kirstein S and M¨ohwald H 1998 *J. Phys. Chem.* B **102** 4096–103
[37] Criste M and Niculescu E C 2012 *Eur. Phys. J.* B **85** 191(2)–191(13)
[38] Wang H, Fang P, Chen Z and Wang S 2007 *Appl. Surf. Sci.* **253** 8495–9
[39] Khanna P K, Singh N and Lumin J 2007 **127** 474–82
[40] Alberti G, Zanoni C, Losi V, Magnaghi L R and Biesuz R 2021 *Chemosensors.* **9** 108(1)–108(26)
[41] Perepelitsa A S, Ovchinnikov O V, Smirnov M S, Kondratenko T S, Grevtseva I G, Aslanov S V and Khokhlov V Y 2021 *J. Lumin.* **231** 117805(1)–117805(9)
[42] Kumari L and Kar A K 2021 *Mater. Lett.* **302** 130398(1)–130398(4)
[43] Ramazanov M A, Hajiyeva F V, Babayev Y A, Valadova G V, Nuriyeva1 S G and Shirinova H A 2020 *J. Elastomers Plast.* **52** 159–66
[44] Su R *et al* 2021 *Nat. Commun.* **12** 2479(1)–2479(11)
[45] Hou X, Kang J, Qin H, Chen X, Ma J, Zhou J, Chen L, Wang L, Wang L-W and Peng X 2019 *Nat. Commun.* **10** 1750(1)–1750(11)
[46] Takagahara T 1993 *Phys. Rev.* B **47** 4569
[47] Radhakrishnan S and Prasanth R 2017 *J. Mater. Sci., Mater. Electron.* **28** 3168–74
[48] Jitianu M and Goia D V 2007 *J. Colloid Interface Sci.* **309** 78–85
[49] Wu L, Yu J C, Zhang L, Wang X and Li S 2004 *J.Solid State Chem.* **126** 3422–3
[50] Wang Z L, Ahmad T S and El-Sayed M A 1997 *Surf. Sci.* **380** 302–10
[51] Qu X, Omar L, Le T B H, Tetley L, Bolton K, Chooi K W, Wang W and Uchegbu I F 2008 *Langmuir* **24** 9997–10004
[52] Ning Z, Tian H, Yuan C, Fu Y, Qin H and Hans A 2011 *Chem. Commun.* 1536–8
[53] Sarah G, Brenda R, John D and Brian N 2007 *Sol. Energy* **81** 540–7
[54] Chen X *et al* 2023 *Nat. Commun.* **14** 284(1)– 284(9)
[55] Cao X, Zheng Z, Zhang Y, Gu G, Miao J, Huang R, Hou B D, Tian Y and Zhang X 2022 *J. Lumin.* **252** 119368(1)–119368(6)
[56] Aleksandrova M 2022 *J. Mater. Sci., Mater. Electron.* **33** 23900–9
[57] Sadeghi E 2009 *Physica E* **41** 1319–22
[58] Bahar M K and Başer P 2022 *The European Physical Journal Plus.* **137** 1138(1)–1138(10)
[59] Maouhoubi I, En-nadir R, Maouhoubi S, Zorkani I, Hassani A O T and Jorio A 2023 *Physica E: Low-dimensional Systems and Nanostructures.* **148** 115630
[60] Yang C C, Liu L C and Chang S H 1998 *Phys. Rev.* B **58** 1954–61
[61] Toscano-Negrett R G *et al* 2023 *Nanomaterials.* **13** 550(1)–550(18)
[62] Hasanirokh K, Radu A and Duque C A 2022 *Nanomaterials.* **12** 4014(1)–4014(14)
[63] Zhen-Yan D *et al* 1994 *Phys. Rev.* B **50** 5736–9
[64] Shi L, Yan Z-W and Wen Meng M 2021 *Superlattices Microstruct.* **150** 106818(1)–106818
[65] Fakkahi A, Jaouane M, Limame K, Sali A, Kirak M, Arraoui R, Ed-Dahmouny A, El-bakkari K and Azmi H 2023 *Appl. Phys.* A **129** 188
[66] M'zerd S, El Haouari M, Aghoutane M, El-Yadri M, Feddi E, Dujardin F, Zorkani I, Jorio A, Sadoqi M and Long G 2018 *J. Appl. Phys.* **124** 164303(1)–164303(8)
[67] Shi L and Yan Z W 2023 *Phys. Lett.* A **466** 128725(1)–
[68] Yesilgul U 2015 *Physica* E **74** 34–8
[69] Rabanian A, Neghabi M, Zadsar M and Jafari M 2021 *Materials Science and Engineering:* B **274** 115489(1)–115489(7)
[70] Zeng Z, Garoufalis C S, Terzis A F and Baskoutas S 2013 *J. Appl. Phys.* **114** 023510(1)–023510(9)
[71] Cheche T O, Barna V and Chang Y C 2013 *Superlattices Microstruct.* **60** 475–86
[72] Shi L and Yan Z W 2016 *Superlattices Microstruct.* **94** 204–14
[73] Aderras L, Bah A, Feddi E, BurileanuF. Dujardin L M and Duque C A 2017 *Physica* E **89** 119–23
[74] Morales A L, Raigoza N, Reyes-Gómez E, Osorio-Guillén J M and Duque C A 2009 *Superlattices Microstruct.* **45** 590–7
[75] Baghramyan H, Barseghyan M, Kirakosyan A A, Restrepo Arango R, Mora-Ramos M and Duque C 2014 *J. Lumin.* **145** 676–83
[76] Cherni A, Yahyaoui N, Zeiri N, Said M and Saadaoui S 2023 *Opt. Quantum Electron.* **55** 273–86
[77] Abed S and Al Rashid S 2019 *AUS.* **26** 53–8
[78] Sandeep V, Sreejith K and Hirendra N G 2013 *J. Phys. Chem.* C **117** 10901–8
[79] Zeiri N, Sfina N, Abdi-Ben Nasrallah S and Said M 2013 *Opt. Mater.* **35** 875–80
[80] Kumar B, Kaushik B K and Negi Y S 2014 *Polym. Rev.* **54** 33–111
[81] Kumar B, Kaushik B K, Negi Y S and Mater J 2014 *Sci: Mater Electron.* **25** 1–30
[82] Zeng Z, Paspalakis E, Garoufalis C S, Terzis A F and Baskoutas1 S 2013 *J. Appl. Phys.* **113** 054303
[83] Shi L, Yan Z-W and Meng M-W 2021 *Superlattices Microstruct.* **150** 106818(1)–106818(10)
[84] Wang G, Zhang L and Wei H 2017 *Adv. Condens. Matter Phys.* **2017** 1–7
[85] Cristea M and Niculescu E C 2012 *The European Physical Journal* B **85** 191(1)–191(13)
[86] Niculescu E C and Cristea M 2013 *J. Lumin.* **135** 120–7

[87] Burileanu L M 2014 *J. Lumin.* **145** 684–9
[88] Shi L and Yan Z W 2018 *Physica* E **98** 111–7
[89] Liang S, Xie W, Li X and Shen H 2011 *Superlattices Microstruct.* **49** 623–31
[90] Barseghyan M G, Mora-Ramos M E and Duque C A 2011 *Eur. Phys. J.* **84** 265–71
[91] Rahmani K, Chrafih Y, M'Zred S, Janati S, Zorkani I, Jorio A and Mmadi A 2018 *J. Phys Conf. Ser.* **984** 012001(1)–012001(8)